Research Article | Vol. 25, No. 10 | 15 May 2017 | OPTICS EXPRESS 10984

Optics EXPRESS

Highly efficient soft X-ray spectrometer based on a reflection zone plate for resonant inelastic X-ray scattering measurements

ZHONG YIN,[1,2,8] JENS REHANEK,[3,9] HEIKE LÖCHEL,[4] CHRISTOPH BRAIG,[5] JENS BUCK,[6] ALEXANDER FIRSOV,[5] JENS VIEFHAUS,[6] ALEXEI ERKO,[5] AND SIMONE TECHERT [1,2,7,10]

[1]*Dept. FS-Structural Dynamics in Chemical Systems, Deutsches Elektronen-Synchrotron (DESY), Hamburg 22607, Germany*
[2]*Structural Dynamics of (Bio)chemical Systems, Max Planck Institute for Biophysical Chemistry, Göttingen 37070, Germany*
[3]*Paul Scherrer Institute, Villigen PSI 5232, Switzerland*
[4]*Neutron Optics Berlin GmbH, Berlin 12489, Germany*
[5]*Helmholtz Zentrum Berlin für Materialien und Energie GmbH, Berlin 12489, Germany*
[6]*FS-PE, Deutsches Elektronen-Synchrotron (DESY), Hamburg 22607, Germany*
[7]*Institute for X-ray Physics, University of Göttingen, 37077 Göttingen, Germany*
[8]*zhong.yin@desy.de*
[9]*jens.rehanek@psi.ch*
[10]*simone.techert@desy.de*

Abstract: We present a newly designed compact and flexible soft X-ray spectrometer for resonant inelastic X-ray scattering (RIXS) studies within an energy range from 380 eV to 410 eV, which would include the K alpha emission lines of vital elements like nitrogen. We utilized an off-axis reflection zone plate (RZP) as the wavelength selective element with a maximum line density of 10000 l/mm. A higher energy resolution over a broader range of ± 15 eV around the designed energy was achieved by displacing the RZP. Additionally, for the first time, an actual optical side effect, the so-called comatic aberration was exploited to increase the energy resolution. First results show a resolving power in the order of 1300 for photon energy of 395 eV, which is comparable to a commercial varied line spacing grating (VLS).

OCIS codes: (300.6560) Spectroscopy, x-ray; (340.7480) X-rays, soft x-rays, extreme ultraviolet (EUV).

References and links

1. L. Ament, M. van Veenendaal, T. Devereaux, J. Hill, and J. van den Brink, "Resonant inelastic x-ray scattering studies of elementary excitations," Rev. Mod. Phys. **83**(2), 705–767 (2011).
2. A. Kotani and S. Shin, "Resonant inelastic x-ray scattering spectra for electrons in solids," Rev. Mod. Phys. **73**(1), 203–246 (2001).
3. J. Schlappa, K. Wohlfeld, K. J. Zhou, M. Mourigal, M. W. Haverkort, V. N. Strocov, L. Hozoi, C. Monney, S. Nishimoto, S. Singh, A. Revcolevschi, J.-S. Caux, L. Patthey, H. M. Rønnow, J. van den Brink, and T. Schmitt, "Spin-orbital separation in the quasi-one-dimensional Mott insulator Sr2CuO3," Nature **485**(7396), 82–85 (2012).
4. M. Lundberg, T. Kroll, S. DeBeer, U. Bergmann, S. A. Wilson, P. Glatzel, D. Nordlund, B. Hedman, K. O. Hodgson, and E. I. Solomon, "Metal-ligand covalency of iron complexes from high-resolution resonant inelastic X-ray scattering," J. Am. Chem. Soc. **135**(45), 17121–17134 (2013).
5. H. Y. Huang, C. J. Jia, Z. Y. Chen, K. Wohlfeld, B. Moritz, T. P. Devereaux, W. B. Wu, J. Okamoto, W. S. Lee, M. Hashimoto, Y. He, Z. X. Shen, Y. Yoshida, H. Eisaki, C. Y. Mou, C. T. Chen, and D. J. Huang, "Raman and fluorescence characteristics of resonant inelastic X-ray scattering from doped superconducting cuprates," Sci. Rep. **6**, 19657 (2016).
6. Z. Yin, I. Rajkovic, S. Thekku Veedu, S. Deinert, D. Raiser, R. Jain, H. Fukuzawa, S. Wada, W. Quevedo, B. Kennedy, S. Schreck, A. Pietzsch, P. Wernet, K. Ueda, A. Föhlisch, and S. Techert, "Ionic Solutions Probed by Resonant Inelastic X-ray Scattering," Z. Phys. Chem. **229**(10-12), 1855–1867 (2015).

#285292 https://doi.org/10.1364/OE.25.010984
Journal © 2017 Received 9 Mar 2017; revised 23 Apr 2017; accepted 23 Apr 2017; published 3 May 2017

Optics EXPRESS

7. M. Agåker, T. Käämbre, C. Glover, T. Schmitt, M. Mattesini, R. Ahuja, J. Söderström, and J.-E. Rubensson, "Resonant inelastic soft x-ray scattering at double core excitations in solid LiCl," Phys. Rev. B **73**(24), 245111 (2006).
8. Z. Yin, I. Rajkovic, K. Kubicek, W. Quevedo, A. Pietzsch, P. Wernet, A. Föhlisch, and S. Techert, "Probing the Hofmeister Effect with Ultrafast Core-Hole Spectroscopy," J. Phys. Chem. B **118**(31), 9398–9403 (2014).
9. P. Wernet, K. Kunnus, I. Josefsson, I. Rajkovic, W. Quevedo, M. Beye, S. Schreck, S. Grübel, M. Scholz, D. Nordlund, W. Zhang, R. W. Hartsock, W. F. Schlotter, J. J. Turner, B. Kennedy, F. Hennies, F. M. F. de Groot, K. J. Gaffney, S. Techert, M. Odelius, and A. Föhlisch, "Orbital-specific mapping of the ligand exchange dynamics of Fe(CO)5 in solution," Nature **520**(7545), 78–81 (2015).
10. J.-E. Rubensson, "Resonant inelastic soft X-ray scattering applied to molecular materials," J. Electron Spectrosc. Relat. Phenom. **200**, 239–246 (2015).
11. Y. Y. Peng, M. Hashimoto, M. M. Sala, A. Amorese, N. B. Brookes, G. Dellea, W.-S. Lee, M. Minola, T. Schmitt, Y. Yoshida, K.-J. Zhou, H. Eisaki, T. P. Devereaux, Z.-X. Shen, L. Braicovich, and G. Ghiringhelli, "Magnetic excitations and phonons simultaneously studied by resonant inelastic x-ray scattering in optimally doped $Bi_{1.5}P_{0.55}Sr_{1.6}La_{0.4}CuO_{6+\delta}$," Phys. Rev. B **92**(64517), 1–8 (2015).
12. M. O. Krause, "Atomic radiative and radiationless yields for K and L shells," J. Phys. Chem. Ref. Data **8**(2), 307–327 (1979).
13. T. Wilhein, D. Hambach, B. Niemann, M. Berglund, L. Rymell, and H. M. Hertz, "Off-axis reflection zone plate for quantitative soft x-ray source characterization," Appl. Phys. Lett. **71**(2), 190–192 (1997).
14. S. G. Chiuzbăian, C. F. Hague, A. Avila, R. Delaunay, N. Jaouen, M. Sacchi, F. Polack, M. Thomasset, B. Lagarde, A. Nicolaou, S. Brignolo, C. Baumier, J. Lüning, and J.-M. Mariot, "Design and performance of AERHA, a high acceptance high resolution soft x-ray spectrometer," Rev. Sci. Instrum. **85**(4), 043108 (2014).
15. Z. Yin, H. B. Peters, U. Hahn, M. Agåker, A. Hage, R. Reininger, F. Siewert, J. Nordgren, J. Viefhaus, and S. Techert, "A new compact soft x-ray spectrometer for resonant inelastic x-ray scattering studies at PETRA III," Rev. Sci. Instrum. **86**(9), 093109 (2015).
16. T. Tanikawa, A. Hage, M. Kuhlmann, J. Gonschior, S. Grunewald, E. Plönjes, S. Düsterer, G. Brenner, S. Dziarzhytski, M. Braune, M. Brachmanski, Z. Yin, F. Siewert, T. Dzelzainis, B. Dromey, M. J. Prandolini, F. Tavella, M. Zepf, and B. Faatz, "First observation of SASE radiation using the compact wide-spectral-range XUV spectrometer at FLASH2," Nucl. Instrum. Meth. **830**, 170–175 (2016).
17. L. Poletto, F. Frassetto, P. Miotti, A. Di Cicco, P. Finetti, C. Grazioli, F. Iesari, A. Kivimäki, S. Stagira, and M. Coreno, "Spectrometer for X-ray emission experiments at FERMI free-electron-laser," Rev. Sci. Instrum. **85**(10), 103112 (2014).
18. O. Fuchs, L. Weinhardt, M. Blum, M. Weigand, E. Umbach, M. Bär, C. Heske, J. Denlinger, Y.-D. Chuang, W. McKinney, Z. Hussain, E. Gullikson, M. Jones, P. Batson, B. Nelles, and R. Follath, "High-resolution, high-transmission soft x-ray spectrometer for the study of biological samples," Rev. Sci. Instrum. **80**(6), 063103 (2009).
19. G. Ghiringhelli, A. Piazzalunga, C. Dallera, G. Trezzi, L. Braicovich, T. Schmitt, V. N. Strocov, R. Betemps, L. Patthey, X. Wang, and M. Grioni, "SAXES, a high resolution spectrometer for resonant x-ray emission in the 400–1600 eV energy range," Rev. Sci. Instrum. **77**, 113108 (2006).
20. Y. Harada, M. Kobayashi, H. Niwa, Y. Senba, H. Ohashi, T. Tokushima, Y. Horikawa, S. Shin, and M. Oshima, "Ultrahigh resolution soft x-ray emission spectrometer at BL07LSU in SPring-8," Rev. Sci. Instrum. **83**(1), 013116 (2012).
21. T. A. Callcott, K. L. Tsang, C. H. Zhang, D. L. Ederer, and E. T. Arakawa, "High-efficiency soft x-ray emission spectrometer for use with synchrotron radiation excitation," Rev. Sci. Instrum. **57**(11), 2680–2690 (1986).
22. J. Nordgren, G. Bray, S. Cramm, R. Nyholm, J.-E. Rubensson, and N. Wassdahl, "Soft x-ray emission spectroscopy using monochromatized synchrotron radiation," Rev. Sci. Instrum. **60**(7), 1690–1696 (1989).
23. https://www.bnl.gov/ps/beamlines/beamline.php?r=2-ID, (2016).
24. https://www.maxiv.lu.se/accelerators-beamlines/beamlines/veritas/, (2016).
25. http://www.esrf.eu/home/UsersAndScience/Experiments/EMD/ID32/RIXS.html, (2016).
26. C. H. Lai, H. S. Fung, W. B. Wu, H. Y. Huang, H. W. Fu, S. W. Lin, S. W. Huang, C. C. Chiu, D. J. Wang, L. J. Huang, T. C. Tseng, S. C. Chung, C. T. Chen, and D. J. Huang, "Highly efficient beamline and spectrometer for inelastic soft X-ray scattering at high resolution," J. Synchrotron Radiat. **21**(2), 325–332 (2014).
27. H. Yamane, N. Kosugi, and T. Hatsui, "Transmission-grating spectrometer for highly efficient and high-resolution soft x-ray emission studies," J. Electron Spectrosc. Relat. Phenom. **188**, 155–160 (2013).
28. T. Tokushima, Y. Horikawa, and S. Shin, "Triple-path collector optics for grazing incident x-ray emission spectrometer," Rev. Sci. Instrum. **82**(7), 073108 (2011).
29. C. Braig, H. Löchel, A. Firsov, M. Brzhezinskaya, A. Hafner, J. Rehanek, M. Wojcik, A. Macrander, L. Assoufid, and A. Erko, "Hard x-ray spectroscopy and imaging by a reflection zone plate in the presence of astigmatism," Opt. Lett. **41**(1), 29–32 (2016).
30. R. Mitzner, J. Rehanek, J. Kern, S. Gul, J. Hattne, T. Taguchi, R. Alonso-Mori, R. Tran, C. Weniger, H. Schröder, W. Quevedo, H. Laksmono, R. G. Sierra, G. Han, B. Lassalle-Kaiser, S. Koroidov, K. Kubicek, S. Schreck, K. Kunnus, M. Brzhezinskaya, A. Firsov, M. P. Minitti, J. J. Turner, S. Moeller, N. K. Sauter, M. J. Bogan, D. Nordlund, W. F. Schlotter, J. Messinger, A. Borovik, S. Techert, F. M. F. de Groot, A. Föhlisch, A. Erko, U. Bergmann, V. K. Yachandra, P. Wernet, and J. Yano, "L-Edge X-ray Absorption Spectroscopy of

Optics EXPRESS

Dilute Systems Relevant to Metalloproteins Using an X-ray Free-Electron Laser," J. Phys. Chem. Lett. **4**(21), 3641–3647 (2013).
31. P. Baumgärtel, M. Witt, J. Baensch, M. Fabarius, A. Erko, F. Schäfers, and H. Schirmacher, "RAY-UI: A Powerful and Extensible User Interface for RAY," AIP Conf. Proc. **1741**, 040016 (2016).
32. http://www.gsolver.com/, (2016).
33. J. Rehanek, F. Schäfers, H. Löchel, A. Firsov, J. Grünert, W. Freund, C. Ozkan, S. Molodtsov, and A. Erko, "A case study of novel X-ray Optics for FEL sources," J. Phys. Conf. Ser. **425**(52013), 1–4 (2013).
34. C. Braig, H. Löchel, J. Rehanek, A. Firsov, M. Brzhezinskaya, and A. Erko, "Reflection zone plate concept for resonant inelastic X-ray scattering spectrometry," Appl. Opt. **56**(3), 515–520 (2017).
35. C. Braig, H. Löchel, R. Mitzner, W. Quevedo, P. Loukas, M. Kubin, C. Weniger, A. Firsov, J. Rehanek, M. Brzhezinskaya, P. Wernet, A. Föhlisch, and A. Erko, "Design and optimization of a parallel spectrometer for ultra-fast X-ray science," Opt. Express **22**(10), 12583–12602 (2014).
36. M. Brzhezinskaya, A. Firsov, K. Holldack, T. Kachel, R. Mitzner, N. Pontius, J. S. Schmidt, M. Sperling, C. Stamm, A. Föhlisch, and A. Erko, "A novel monochromator for experiments with ultrashort X-ray pulses," J. Synchrotron Radiat. **20**(4), 522–530 (2013).
37. J. Viefhaus, F. Scholz, S. Deinert, L. Glaser, M. Ilchen, J. Seltmann, P. Walter, and F. Siewert, "The Variable Polarization XUV Beamline P04 at PETRA III: Optics, mechanics and their performance," Nucl. Instrum. Methods Phys. Res. A **710**, 151–154 (2013).
38. Z. Yin, H.-B. Peters, U. Hahn, J. Gonschior, D. Mierwaldt, I. Rajkovic, J. Viefhaus, C. Jooss, and S. Techert, "An endstation for resonant inelastic X-ray scattering studies of solid and liquid samples," J. Synchrotron Radiat. **24**(1), 302–306 (2017).

1. Introduction

Resonant inelastic X-ray scattering (RIXS) has become a popular tool to study the element-specific electronic structure of complex systems in hard and soft condensed matter or in chemical reactions. This photon-based method is bulk, element, orbital and site specific as well as polarization sensitive [1,2]. Published results cover a broad range of scientific fields including e.g. charge transfer, electron-phonon interaction and samples in liquid state among others [1–11]. A critical aspect of the RIXS method is the low cross section for the radiative decay channel after core-ionization for light elements [12]. Light elements, however, are the building blocks of all compounds relevant in biology and life research. Additionally, the detection efficiency of soft X-ray spectrometers is also low due to grazing incidence gratings and long distances between source and optical element, which lead to a very small solid angle [13–15]. This results in a need for brilliant light sources. Soft X-ray spectrometers based on gratings in Rowland circle design or varied line spacing gratings are well-established instrumentation around the world [11–27]. Depending on the experimental requirements, some reach theoretically high resolution up to $E/\Delta E = 10^5$. However, these are very large instruments with up to 15 m arm length [14,19,20,22–26]. Other spectrometer designs use additional optical elements to increase the solid angle, e.g. a Wolter type I or a set of collecting mirrors before the diffraction optics [27,28]. Yet, the optimization becomes time consuming and theses devices are usually permanent end stations, which are not suited for a flexible spectrometer.

In this work, we present for the first time soft X-ray emission spectroscopy measurements utilizing a RZP. It uses only one optical element for focusing and diffraction. It combines a mobile and compact design with large solid angles and medium energy resolution in the range of 0.3 eV at 395 eV making it ideal for the study of systems in low amounts (such as typical chemical or biochemical samples).

In previous studies, reflection zone plates (RZP) have been utilized for hard X-ray [29] and for soft X-ray absorption spectroscopy measurements [30]. Yet, the latter suffers from a very low energy resolution. The advantage of RZP for the X-ray absorption studies is the high detection efficiency [30].

To compensate the weakness of RZPs (the limited energy range of nearly maximum resolving power, if the detector is placed perpendicular to the optical axis) we propose to elongate the source RZP distance to achieve a more homogenous energy resolution over a larger energy range. Figure 1 summarizes the calculated and experimental determined resolving power for the designed geometry in comparison to the misaligned configuration. For

Optics EXPRESS

the simulation, two different programs were utilized, RAY [31] for simulating the energy resolution and a grating analyses tool for the efficiency calculation [32].

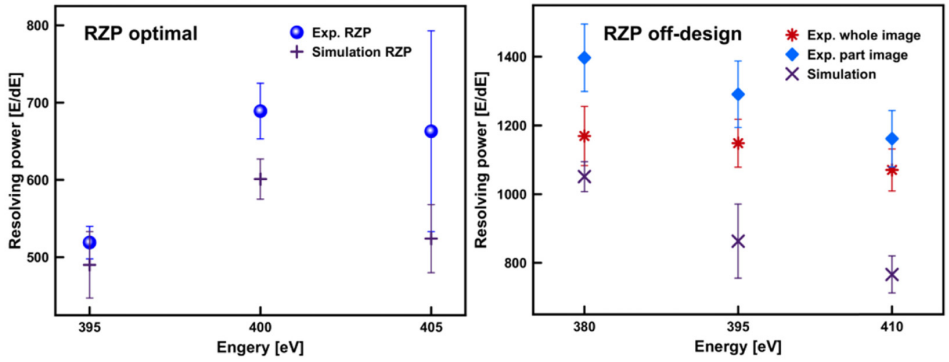

Fig. 1. Left: The energy resolving power simulated for the designed geometry in comparison to the experimental data. Right: Simulated and experimental data for the resolving power with an elongated source RZP distance. The resolving power decreases significantly for energies above and below 400 eV in the optimal geometry case, while it stays more homogenous for the off-design configuration. The experimental and calculation conditions are described in sections 2 and 3.

2. Optical and instrumental design

This part describes the development of the high throughput reflection zone plate (RZP) spectrometer for X-ray emission detection at the nitrogen K-edge (395 eV). One of the technical needs for this spectrometer includes the largest possible solid angle, as the intensity of energy to be measured is expected to be very low – due to the low cross section of the radiative decay channel. Such an arrangement allows reaching the highest possible share of photons and to measure with the highest possible energy resolution at the same time. We decided to make use of a RZP structure, based on our experience with the application of RZP for detection of the weak fluorescence signal of a single element and the RZP's potential to deliver very high energy resolution measurements data [33–35].

In previous studies, an array of RZP structures were designed for a perfect focus of the same photon energy on a line or row of spots in order to have as much surface area covered with highly efficient diffracting structure as possible [30,33–35].

In the present case, we opted for a single RZP-structure, as broad as the fabrication limit allows (see Fig. 2). This means, the tiniest structures manufactured are of 100 nm size. This allows for a line density as high as 10000 lines/mm on the outer areas. Restraining the view to the plain number of line density would lead to effectively low efficient optics. In this case, the effective line density is designed from the point of view of the incoming photons. The incident angle is different at the peripheral area compared to the designed central line. The simulation results concerning the effective line density (in the order of 1200 l/mm in the center area and 2200 l/mm at the edges) and the expectable efficiency in these different areas show a decrease in the zone plate areas further away from the source. More precisely, an efficiency loss occurs along the incoming beam, see Fig. 2. Hence, according to our simulations, the benefit of making use of a single RZP-structure is equivalent to an increase of the solid angle by the factor two, compared to a possible array of RZPs – all of them manufactured for the design-energy, taking simply the geometrical configuration of direct line between the source, diffraction area on the RZP, and detector size. The efficiency loss along the optical element from the front to the back is rooted in the different incidence and exit angles along the entire length.

Optics EXPRESS

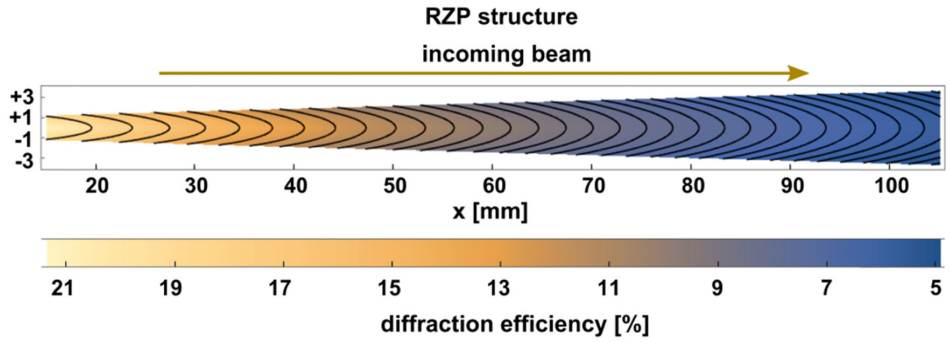

Fig. 2. Efficiency simulation of the entire optical element at the different parts of the structure. It can clearly be seen that the diffraction efficiency drops along the axis of the incoming beam (longitudinal direction). The data was simulated using rigorous couple wave analysis software [32].

According to Fig. 2 it can clearly be seen that the diffraction efficiency drops along the optical axis of the incoming beam, whereas in lateral direction the drop is rather marginal. The reason of this flux difference is mainly due to different distances between source and position on the grating. A simulation of the optimum depth of profile for highest possible efficiency (including Nickel-coating for increased optimal reflectivity at the used angles and photon energy) shows that the integrated efficiency over the entire optical element along the center line is about 12.8 ± 0.1% in case of using the + 1st order of diffraction at 395 eV. Given the RZP parameters as in Table 1, we decided to manufacture the RZP at a constant depth of 10 nm. The vertical acceptance of the RZP is 2.7° and 3.1° in the horizontal direction at an optimal incident angle of 2°, see Fig. 3.

Table 1. The essential designed parameters of the RZP. α and β are the design angles with respect to the center of the RZP structure.

Design energy	**395 eV**
Central line density	**1763 l/mm**
Incident angle **α**	**2°**
Diffraction angle **β**	**6.35°**
Incident arm length $\mathbf{R_1}$	**90 mm**
Exit arm length $\mathbf{R_2}$	**1000 mm**
Reflection coating	**Ni 30 nm**
Micro roughness (rms)	**< 0.6 nm**

Optics EXPRESS

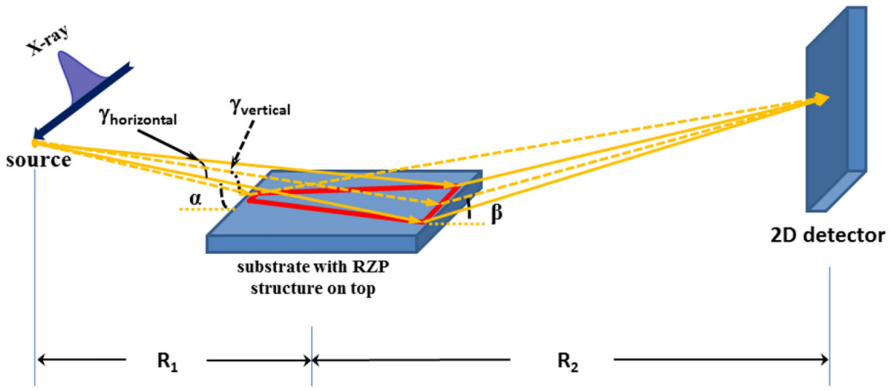

Fig. 3. The geometrical dimensions with the incident (**α**) and diffraction (**β**) angles as well as the vertical ($\gamma_{vertical}$) and horizontal ($\gamma_{horizontal}$) acceptance angles are depicted. The distance from source to RZP is $\mathbf{R_1}$ = 90 mm for the designed geometry or $\mathbf{R_1}$ = 200 mm for the "misaligned" and from the RZP to the 2-D detector ($\mathbf{R_2}$) is 1000 mm. The spectrometer is placed perpendicularly to the incoming X-ray beam, the same applies to the detector in relation to the outgoing beam.

It has been demonstrated from experiments and simulations that a spectrometer equipped with the translational correction of the Cartesian three-dimensional degrees of freedom is sufficient for practical corrections in order to cope with an angular displacement of the RZP. Hence, our spectrometer allows for motorized linear alignment of all three dimensions but does not include rotational movements.

The most critical parameters are the source to RZP (R_1), RZP to detector (R_2) distances, detector height and the incident angle. Based on the optical design of the RZP the source sample distance is 90 mm and the detector is optimally placed 1000 mm away from the RZP. The optimal incidence angle for the designed energy of 395 eV is at 2° to allow a high efficiency of diffraction. In this proof of principle experiment the source to RZP distance has been increased to 200 mm. In this actual misalignment, the focal spot is enlarged both vertically and horizontally to a broad and wide bent line. In horizontal direction though (here the dispersive direction), the so-called coma effect comes into play, resulting in a very high concentration of intensity only at the upper edge of the focal area. This intensity concentration is so narrow that it can be treated as the focal line of a very small width. As shown below, this width remains small within a wide energy range. Of course, the increased distance, a misalignment from design parameters, leads to a decrease of the horizontal acceptance angles to 1.7° and vertical acceptance to 0.95°.

The spectrometer is motorized to achieve the optimal position and high reproducibility of the optical element for a high efficiency with sufficient energy resolution of 0.3 eV at 395 eV, which is comparable to existing grating spectrometers [15,17,22].

The behavior of an RZP structure along the optical axis is exactly the same as a conventional VLS grating manufactured on a plane substrate. The groove density variation along the optical axis (x-axis) can be described with this equation:

$$\frac{1}{d(x)} = \frac{1}{\lambda}\left\{\cos\left[\alpha\tan\left(\frac{R_1\sin\alpha}{R_1\cos\alpha - x}\right)\right] - \cos\left[\alpha\tan\left(\frac{R_2\sin\beta}{R_2\cos\beta + x}\right)\right]\right\}, \qquad (1)$$

where d(x) is in the local grating period in optical axis direction and all other terms correspond according to Table 1. The angles α and β are connected to each other by the grating equation:

$$d(\cos\alpha - \cos\beta) = n\lambda. \qquad (2)$$

Optics EXPRESS

It can easily be seen that for any wavelength by varying parameters α, R_1 and R_2 one can optimize the desired line density profile on the grating. It will give maximum energy resolving power on any wanted wavelength different from the RZP design energy.

A silicon wafer serves as substrate with a liquid photo resist, for example, the positive resist polymethyl methacrylate, spin-coated onto it. After coating, the wafer is baked on a hotplate, in order to vaporize the remaining solvent. Afterwards, the e-beam writer (VISTEC EBPG 5000 + , running at an accelerating voltage of 100 kV) is used to write the designed structure. Subsequently, the resist is developed. The long and stable carbon-chains are destroyed (cracked) during the interaction with radiation and are dissolved into the developing solvent. In the next step, the structure is etched into the silicon substrate via reactive ion-etching, which is best described as a combination of both physical and chemical etching. After the ion-etching, the remaining resist is removed, leaving a clean silicon surface, structured with lines and spaces as designed. A more detailed description about the manufacturing process can be found in [36].

In the following section, the results of the RZP spectrometer will be compared with a spectrometer equipped with a standard commercially available VLS grating [15]. An Andor iKON M CCD with 1024 x 1024 pixels and a pixel size of 13 x 13 μm^2 has been utilized as a 2D X-ray detector for the RZP as well as the VLS spectrometer.

3. Results and discussion

The measurements utilizing VLS and RZP optics have been performed at the soft X-ray beamline P04 at the synchrotron facility PETRA III at DESY Hamburg, Germany with the ChemRIXS endstation [37,38]. Both spectrometers have been installed perpendicularly to the incoming beam, see Fig. 2. The elastic scattering signals have been used for the energy calibration as well as for the energy resolution studies, because this offers the advantage to know both the energy value and the energy bandwidth of the incoming beam with great precision [37]. The 2D detector is placed perpendicularly to the outgoing optical axis. Figure 4 shows a typical RZP image for an energy range from 375 eV – 415 eV in 5 eV steps for the RZP aligned to the designed geometrical parameter. The acquisition time for each energy was 20 s. For an energy higher than the designed energy, the resolution is higher in comparison to the lower energies. The incident angle deviated slightly from the optimal 2°, which explains why the vertically sharpest signal was recorded at 400 eV and not at 395 eV. The actual incident angle is smaller than 2° due to a larger energy resolution behavior for higher energies. From the simulation, the incident angle was determined to be 1.975°. It is obvious that the energy resolution is not homogenous for an energy range of 40 eV. The corresponding resolving power is illustrated in Fig. 1 left.

In another row of measurements, the source RZP distance was increased to 200 mm to compensate this typical effect utilizing a RZP.

Optics EXPRESS

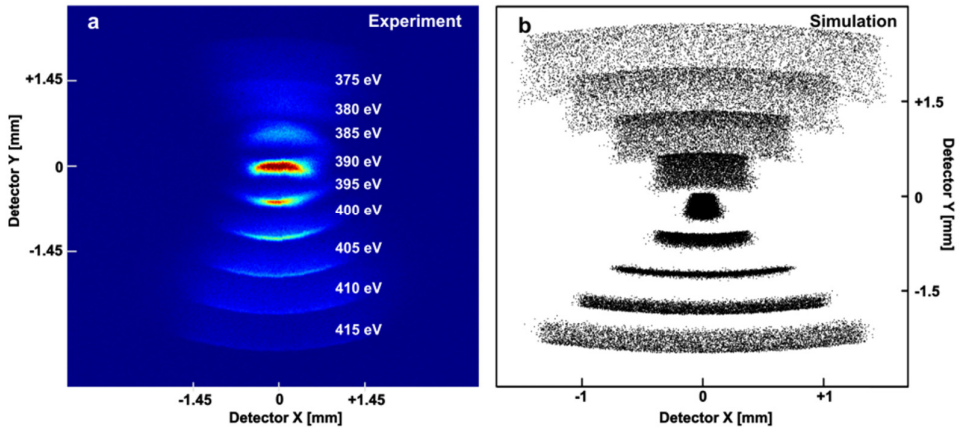

Fig. 4. A sum image for an energy range from 375 eV – 415 eV in 5 eV steps with an acquisition time of 20 s each is displayed in a. The energy resolution is better for energies higher than the designed energy. b shows the simulated data for the same energy steps with an incident angle of 1.975°. There is a good agreement between experiment and simulation.

Figure 5 shows the obtained data from three exposures (at 380 eV, 395 eV and 410 eV) on the left, and the simulated 2D data using a ray tracing program [31] on the right. In this off-geometry (the incoming angle was kept at the design angle of 2°), due to aberrations, the concentration of photon intensity at the outer edge of the focal image is very high. This coma effect results in a pseudo-line-shaped focus with an asymmetric blur of the intensity distribution in the focal plane, characterized by a long "tail" of diffusely scattered photons on the high energy side as shown in the simulation.

The common definition of the spectral resolution by the FWHM ("full width at half maximum") of an e.g. Gaussian or Lorentzian response function fails in this situation but can be overcome by an appropriate cutoff noise level that sets all pixel entries less than this cutoff level to zero across the detector array.

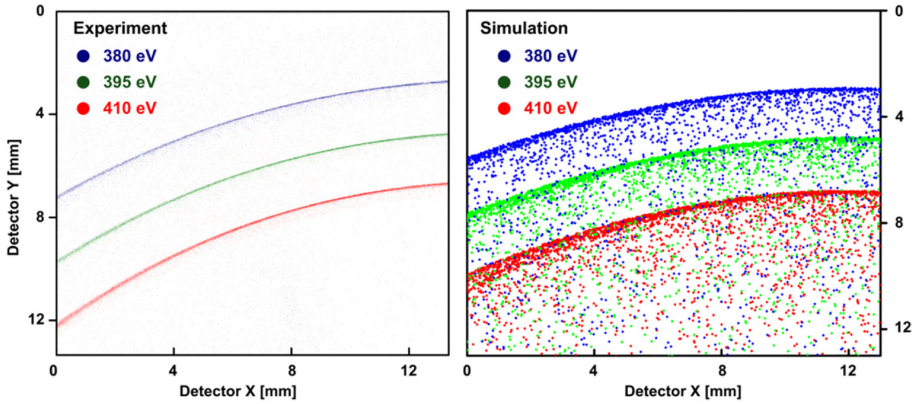

Fig. 5. Left: Signals of 380 eV, 395 eV and 410 eV at a larger source-RZP than the designed distance. The emission lines are recorded all over the CCD detector. Right: Simulated signal for 380 eV, 395 eV and 410 eV. As expected the signal shows strong comatic aberrations.

Depending on the actual peak intensity, this operation shrinks the statistical uncertainty of the photon distribution along the dispersion direction. Transferred to the energy scale, the effective resolution will improve. For the sample energies, we calculate the standard deviation ($\pm \sigma$) as a function of the cutoff level, as shown in Fig. 6.

Optics EXPRESS

Since the peak intensity increases with the energy in this example from 1.6×10^3 at 380 eV to 4.1×10^3 at 410 eV, the standard deviation for each filter level varies, too – a feature which demonstrates the need for a careful calibration of the spectrometer. However, σ falls down rapidly in each case to sub-eV values above a cutoff around 20.

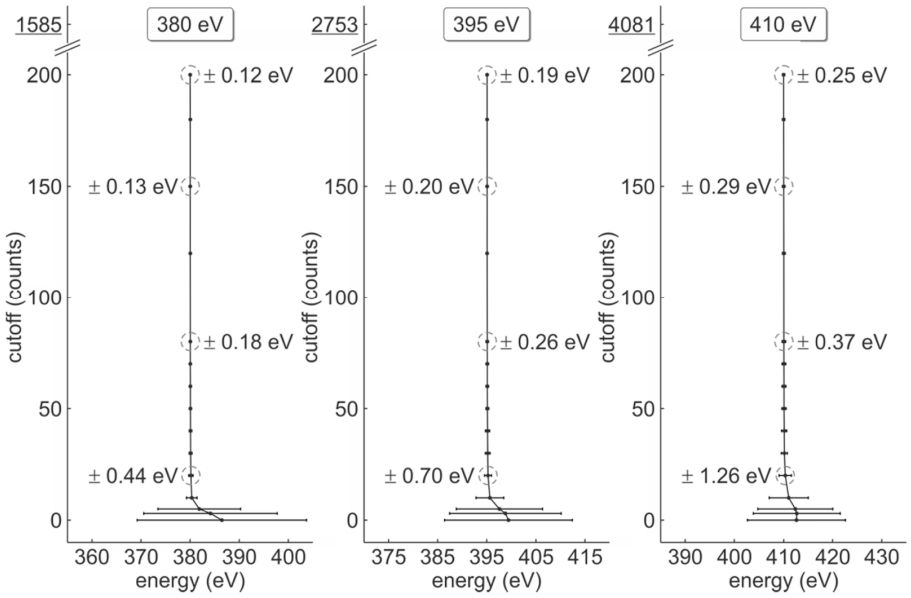

Fig. 6. Standard deviation ("error bars") of the photon distribution on the energy scale for various cutoff levels between 0 and 200 counts. Some values are given as "± (.) eV" data for illustration. Note the different peak intensity in units of counts (underlined number on ordinate axis).

Beyond a cutoff in the order of 50 – 100, the spectral line shape turns into a well-defined, symmetric profile. Such data can be properly fitted by a pseudo-Voigt, here in terms of an equally weighted (50/50) linear combination of a Lorentzian and Gaussian function. In this regime, the mathematical quantity "standard error" may be replaced by the physical FWHM, approaching (0.26 – 0.36) eV toward a filter level of 200. A cut-off level of 60 was used for the data shown in Fig. 7 and 8.

The signal is recorded all over the detector image. The simulated results can reproduce the experimental data (left) very well in terms of energy resolution, dispersion and curvature. The focal intensity distribution is more widely extended than the detector size, which means that only a fraction of the signal is recorded. By increasing the source-optic distance, the focusing characteristics approximate a VLS grating. Having a larger detector screen, a broader part and hence more signal could be recorded.

Figure 7 shows the curvature corrected 1D spectra recorded with the RZP (bottom) for the designed energy of 395 eV and ± 15 eV. The signal is the elastic scattering of a carbon sample, and the beamline energy resolving power was set to ~0.2 eV. The total data acquisition time was 5 min.

The X-ray spot had a linear focus with a dimension of ~20 µm x 170 µm, which is optimized for a liquid jet as the sample delivery system. The X-ray spot size is the source size. An efficiency difference using the RZP is observable between 380 eV and 410 eV.

Since the incident angle is not optimal, the outcome is an increase of scattered photons. This can be suppressed by increasing the cut off of the noise level.

The spectra taken with the RZP are fitted with a Voigt profile. The Voigt shape results from the fact that the beamline itself contributes a Gaussian energy profile in first approximation while the coma aberrations of the spectrometer in this case distort it in a more

Optics EXPRESS

Lorentzian-like manner. The Gaussian part is determined by the beamline energy resolution and has been kept fixed in the fitting process. The total energy resolution is 0.32 eV at 380 eV, 0.35 eV at 395 eV and 0.38 eV at 410 eV.

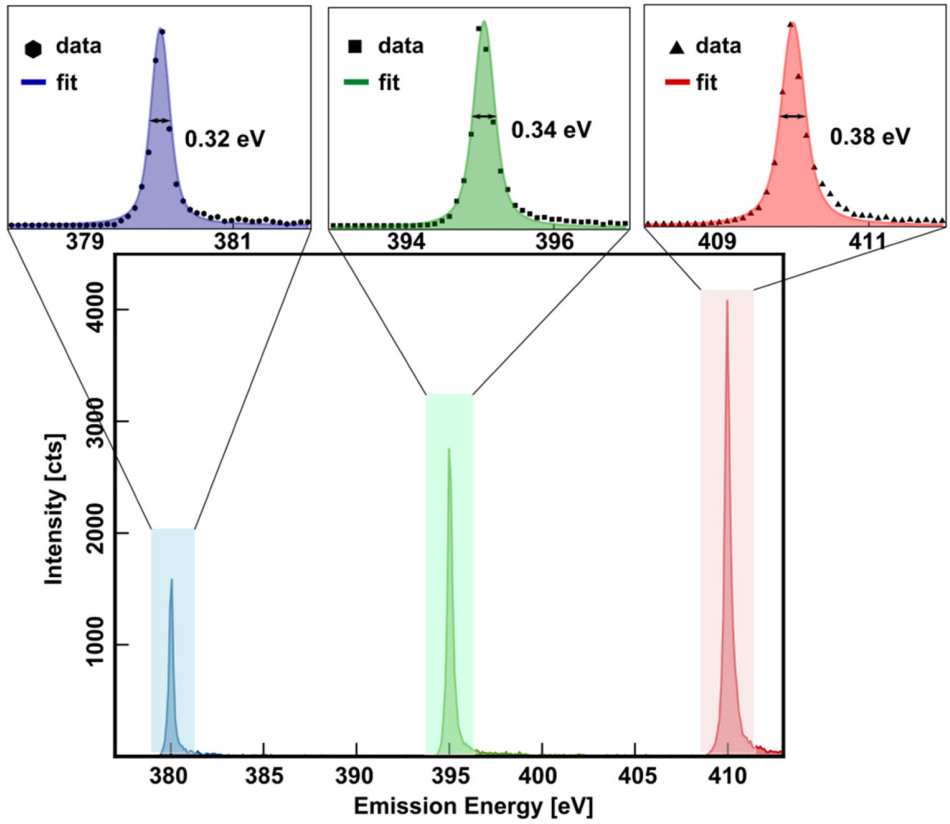

Fig. 7. The bottom spectrum shows the three energies at 380 eV, 395 eV (designed) and 410 eV recorded with the RZP as the optical element. In the upper part, each energy is displayed with a Voigt-fit and the energy resolution.

As displayed in Fig. 5 the edges of the screen show a broadening behavior due to aberrations, therefore we expect a better energy resolution around the middle of the screen. In Fig. 8, a part around the middle with a width of ± 1.45 mm horizontally is summed up compared to the whole detector area.

Optics EXPRESS

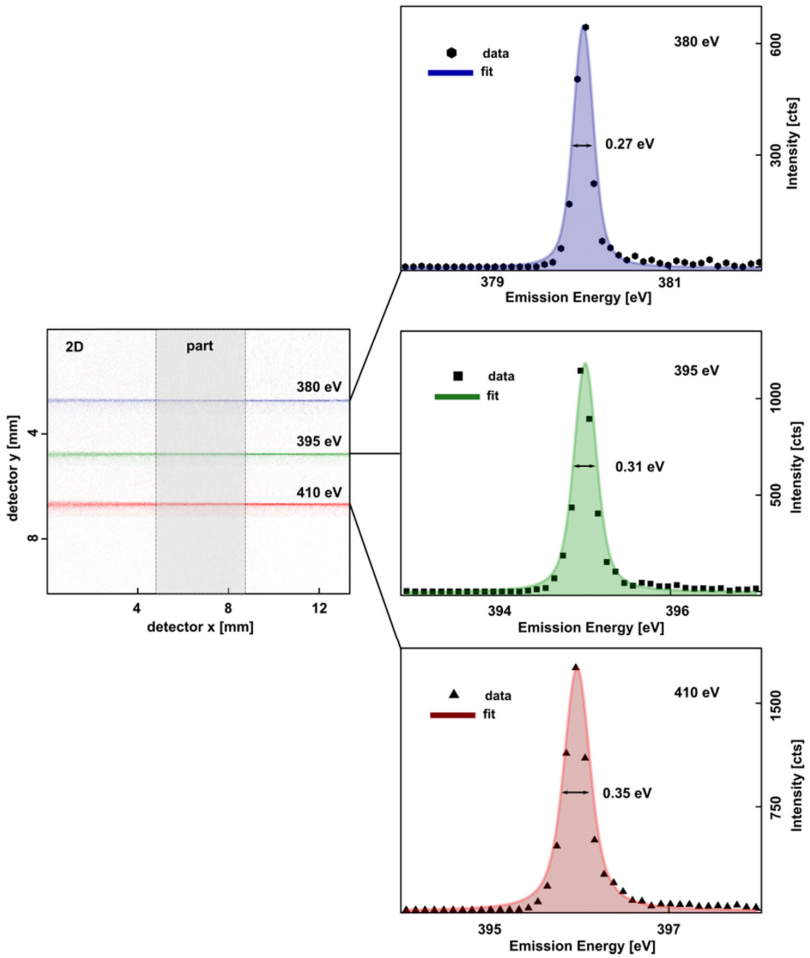

Fig. 8. Left: the curvature corrected 2D image of the detector with the partial cut used for the 1D plot. Right: the 1D plots with the Voigt-fit.

The energy resolution for all three energies increases significantly but the intensity drops down to a third.

In the next step the energy resolution and the efficiency will be compared to a commercially available VLS grating. The spectrum recorded with the VLS grating is fitted using a Gaussian. The essential parameters of the VLS grating are listed in Table 2 from [15].

Table 2. The essential parameters of the VLS grating[a].

Design energy	**210 - 1250 eV**
Central line density	**2400 l/mm**
Incident angle **α**	**1°**
Curvature radius	**58542 mm**
Incident arm length $\mathbf{R_1}$	**564 mm**
Exit arm length $\mathbf{R_2}$	**564 mm**
Reflection coating	**gold**
Slope error (rms)	**2.2 arc sec**

[a]From Rev. Sci. Instrum., **86**, 093109 (2015)

Optics EXPRESS

Figure 9 shows the summed up spectrum of 395 eV taken with the VLS spectrometer and the Gaussian fit. The total energy resolution (ΔE_{total}) is 0.4 eV, which is the combined energy resolution of the spectrometer and beamline $(\Delta E_{beamline})$

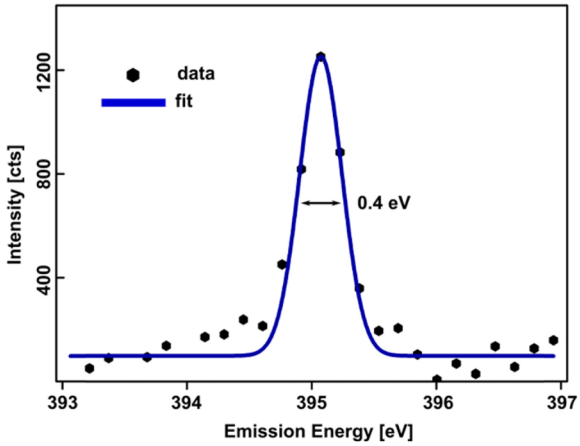

Fig. 9. The Gaussian fit (blue) of the elastic peak (dots) shows a total energy resolution of 0.4 eV at 395 eV recorded with a VLS spectrometer.

In first approximation, the beamline has a Gaussian profile. Therefore, the effective energy resolution of a spectrometer (ΔE_{eff}) can be obtained from this equation:

$$\left(\frac{\Delta E_{eff}}{E}\right) = \sqrt{\left(\frac{\Delta E_{total}}{E}\right)^2 - \left(\frac{\Delta E_{beamline}}{E}\right)^2}. \quad (3)$$

In the case of the VLS spectrometer, the energy resolution (ΔE_{eff}) is 0.34 eV, which corresponds to an energy resolving power of ~1160 (E/ΔE). The resolving power could be higher if the effective pixel size of the detector were smaller. According to manufacturer of the CCD the pixel size is 13 x 13 μm^2, but due to charge spreading the effective size is 26 µm or bigger resulting in a lower energy resolution [15]. For the RZP spectrometer the charge spreading of the CCD has less influence on the energy resolution, due to geometrical configuration. A comparison with the RZP shows that the intensity is a factor of ~3 higher than the VLS spectrometer. This drops down for the partial RZP signal. The efficiency differences are due to the facts of i) Ni-coating of the RZP structure and ii) the VLS optic being positioned by a factor of 2.8 further away from the source. In optimal geometry the intensity increases to more than an order of magnitude for the design energy due to the very large solid angle while maintaining a comparable energy resolution, see also Fig. 2. The energy range of the RZP is limited in detecting the emission line of one element, while the VLS grating offers the possibility to measure the emission lines of up to three different elements [15]. This weakness can be overcome using a target holder with multiple ports for several RZP optics. Another approach would be to implement more than one array on the substrate to cover the emission lines of other elements. Also, the utilized VLS grating reported in this paper is a standard grating with potential of improving performances, e.g. a better energy resolution and higher efficiency can be reached by optimizing the slope error and the coating. Compared to other solutions using a VLS-grating, it is possible to get much closer to the sample with an RZP than with the presented VLS-geometries.

The RZP can be designed for higher energy resolution, standing very close to the source (sample). In this proof-of-principle study the RZP is designed for a nominal distance of

Optics EXPRESS

90mm, but used at a distance of 200mm. These distances can be even shortened, which leads to a remarkably greater solid angle and therefore an increase of the detection efficiency without additional collecting optics. We are using the principle of getting as close as possible to the source, in order to increase the number of collected photons, and at the same time to keep a certain distance to the detector, in order to have reasonable energy resolution. In future studies, these parameters can be optimized. This means shortening the distance source-RZP, and at the same time elongating the RZP-detector distance. Our goal was and is to provide a compact and versatile device, but for a fixed end station these parameters would certainly have to be optimized.

Nevertheless, the presented results utilizing a RZP optic show comparable energy resolution at higher efficiency and may be a candidate for alternative solutions of X-ray optics.

4. Conclusion

We presented a novel approach for soft X-ray emission spectroscopy with reflection zone plates and utilized usually unwanted comatic aberrations to increase the energy resolution for a broader energy range. On one hand in the designed geometry the RZP offers optimal performance in terms of very high efficiency and signal to noise ratio for the set energy. On the other hand the conventional use of RZPs lacks insufficient energy resolution for a wide energy range. Our approach shows that these characteristics can be overcome through displacement of the optic. The results show an energy resolving power of up to ~1300 for an energy range of 30 eV around the nitrogen edge with a much higher efficiency than conventional optics. Spectrometer based on the RZP might offer an alternative instrumental approach for soft RIXS experiments.

Funding

German Research Foundation: SFB755 “Nanoscale Photonic Imaging” Project No. B03 and Project No. C02 of SFB 1073 “Atomic Scale Control of Energy Conversion”; Max Planck Institute of Biophysical Chemistry. Helmholtz Society (POF III/MML-RT5).

Acknowledgments

We thank the staff of P04, the DESY workshops and computing for their continuous support.